Write-error rate of nanoscale magnetic tunnel junctions in the precessional regime

著者	Takaharu Saino, Shun Kanai, Motoya Shinozaki, Butsurin Jinnai, Hideo Sato, Shunsuke Fukami, Hideo Ohno
journal or publication title	Applied physics letters
volume	115
number	14
page range	142406-1-142406-5
year	2019-10-01
URL	http://hdl.handle.net/10097/00130906

doi: 10.1063/1.5121157

Applied Physics Letters

Write-error rate of nanoscale magnetic tunnel junctions in the precessional regime

Cite as: Appl. Phys. Lett. **115**, 142406 (2019); https://doi.org/10.1063/1.5121157
Submitted: 22 July 2019 . Accepted: 19 September 2019 . Published Online: 01 October 2019

Takaharu Saino, Shun Kanai, Motoya Shinozaki, Butsurin Jinnai, Hideo Sato, Shunsuke Fukami, and Hideo Ohno

Applied Physics Letters ARTICLE scitation.org/journal/apl

Write-error rate of nanoscale magnetic tunnel junctions in the precessional regime

Cite as: Appl. Phys. Lett. **115**, 142406 (2019); doi: 10.1063/1.5121157
Submitted: 22 July 2019 · Accepted: 19 September 2019 ·
Published Online: 1 October 2019

Takaharu Saino,[1] Shun Kanai,[1,2,a)] Motoya Shinozaki,[1] Butsurin Jinnai,[3] Hideo Sato,[1,2,4,5] Shunsuke Fukami,[1,2,3,4,5] and Hideo Ohno[1,2,3,4,5]

AFFILIATIONS

[1]Laboratory for Nanoelectronics and Spintronics, Research Institute of Electrical Communication, Tohoku University, Sendai 980-8577, Japan
[2]Center for Spintronics Research Network, Tohoku University, Sendai 980-8577, Japan
[3]WPI-Advanced Institute for Materials Research, Tohoku University, Sendai 980-8577, Japan
[4]Center for Innovative Integrated Electronic Systems, Tohoku University, Sendai 980-0845, Japan
[5]Center for Science and Innovation in Spintronics, Tohoku University, Sendai 980-8577, Japan

[a)]**Author to whom correspondence should be addressed:** sct273@riec.tohoku.ac.jp. **Tel.:** +81-22-217-5555. **Fax:** +81-22-217-5555.

ABSTRACT

We investigate the write-error rate (WER) of spin-transfer torque (STT)-induced switching in nanoscale magnetic tunnel junctions (MTJs) for various pulse durations down to 3 ns. While the pulse duration dependence of switching current density shows a typical behavior of the precessional regime, WER vs current density is not described by an analytical solution known for the precessional regime. The measurement of WER as a function of magnetic field suggests that the WER is characterized by an effective damping constant, which is significantly larger than the value determined by ferromagnetic resonance. The current density dependence of WER is well reproduced by a macrospin model with thermal fluctuation using the effective damping constant. The obtained finding implies a larger relaxation rate and/or thermal agitation during STT switching, offering a previously unknown insight toward high-reliability memory applications.

Spin-transfer torque (STT)-induced magnetization switching in nanoscale magnetic tunnel junctions (MTJs)[1–4] is a key ingredient for magnetoresistive random access memories (MRAMs), which have started to be commercialized recently. While the first generation STT-MRAMs will replace a part of embedded flash memories, much effort is now devoted to the application of STT-MRAMs as cache memories, where the write-error rate (WER) in the high-speed (∼nanoseconds) regime is one of the most critical indices. The WER is also an interesting subject in fundamental research since it relates to the dynamics of collective spin systems under an interplay of energy relaxation, thermal fluctuation, and STT. To date, a number of studies on WER have been reported; analytical formulation and numerical calculation were carried out,[5–8] while WER was measured as a performance index of integrated MTJs in test chips.[9–12]

It is known that there are two regimes of STT switching depending on the time scale: thermally activated regime and precessional regime.[13] For current pulses with duration τ longer than several tens of nanoseconds, the switching probability, or WER, obeys the Arrhenius law against an effective energy barrier modified by the external magnetic field and/or STT, falling into the thermally activated regime, where critical current linearly increases with decreasing log τ.[7] On the other hand, in the precessional regime for τ shorter than several nanoseconds, switching/nonswitching is determined by the total amount of transferred angular momentum, leading to a linear relationship of the switching current with $1/\tau$. The analytical solution of WER in the precessional regime is derived by considering the dispersion of the initial magnetization angle due to the thermal fluctuation (described later for more details). However, it has not been clarified how accurately this solution describes the experimental results and what factors fill the gap between the model and experiment if any. In this paper, we measure WER of nanoscale MTJs by nanosecond pulses under various magnetic fields and discuss the mechanism of WER through a comparison of experimental results with the analytical solution and numerical simulation.

A standard stack structure for high performance MTJs, Ta (5 nm)/Pt (5 nm)/[Co (0.4 nm)/Pt (0.4 nm)]$_{\times 6}$/Co (0.4 nm)/Ru (0.4 nm)/[Co (0.4 nm)/Pt (0.4 nm)]$_{\times 2}$/Co (0.4 nm)/Ta (0.2 nm)/$Co_{0.19}Fe_{0.56}B_{0.25}$ (1 nm)/MgO/$Co_{0.19}Fe_{0.56}B_{0.25}$ (1.6 nm)/Ta (0.2 nm)/$Co_{0.19}Fe_{0.56}B_{0.25}$ (1 nm)/MgO/Ru (5 nm)/Ta (50 nm), is fabricated on a sapphire substrate by dc/rf magnetron sputtering. The bottom CoFeB coupled with a synthetic ferrimagnetic structure through Ta (0.2 nm) corresponds to the reference layer, whereas CoFeB (1.6 nm)/Ta (0.2 nm)/CoFeB (1 nm) corresponds to the free layers with a double MgO interface.[14] Both the reference and free layers possess a perpendicular easy axis. The stack is processed into MTJs with electron-beam lithography, reactive-ion etching, and Ar-ion milling. We fabricate MTJ devices with a coplanar waveguide made of Cr (5 nm)/Au (100 nm) on a sapphire substrate for the high-frequency measurement. After processing, MTJs are annealed at 300 °C for 1 h in vacuum under a perpendicular magnetic field of 0.4 T. The resistance area product RA is determined to be 2.9 $\Omega\mu m^2$ from a linear relationship between R^{-1} and A for MTJs with diameter $D > 37$ nm, where A is measured using a scanning electron microscope. The effective diameter of each MTJ is electrically determined from the above RA and measured R. In this paper, we focus on an MTJ with $D = 24$ nm, where WER for 50-ns pulses is confirmed to be well described by an analytical solution of a thermally activated regime with a macrospin approximation (see the supplementary material).

The WER is measured by using an electrical circuit shown in Fig. 1(a). Positive voltage is defined as a direction where electrons flow from the free layer to the reference layer. We apply a 100-μs-long waveform 1.6×10^4 times using an arbitrary waveform generator (AWG), where the unit waveform consists of initialization, write, and read pulses as shown in Fig. 1(b). The amplitude and duration of the write pulses (V_{write}, τ) are varied, whereas those for initialization and reading are fixed at (420 mV, 6 μs) and (−90 mV, 60 ns), respectively. A high-speed oscilloscope records the transmitted voltage for each read pulse of 100-μs-long waveform, i.e., generating a histogram of 1.6×10^4 results. Examples of histograms for a series of current densities J are shown in Figs. 1(c)–1(f), indicating an increase in switching probability from conductive parallel (P) to less conductive antiparallel (AP) states with increasing J. The magnitude of J is determined from the transmitted voltage $V_{T,write}$ for write voltage: $J = V_{T,write}/AZ_0$, where Z_0 is the characteristic impedance 50 Ω. WER is calculated by the number of unswitched events divided by total trials. Standard deviations of the transmitted voltage $V_{T,read}$ for read voltage for P and AP

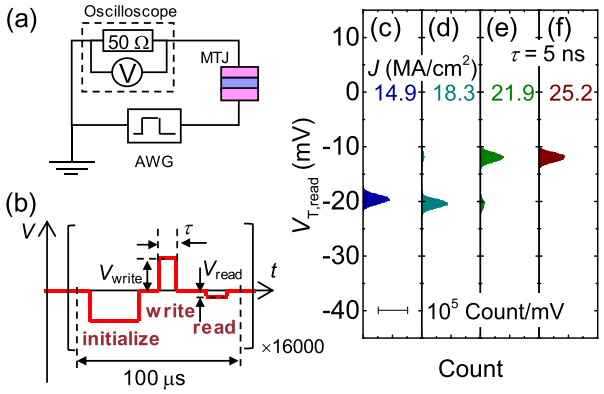

FIG. 1. Schematic diagram of (a) measurement setup and (b) applied pulse voltage waveform. (c)–(f) Histogram of transmitted voltage $V_{T,read}$ for 1.6×10^4 trials with different current densities J.

states are almost identical, and the ratio of the peak-to-peak distance to the deviations is ∼9, which is large enough to discuss WER down to $\sim 3 \times 10^{-6}$. The entire measurement including the creation of the histogram for one set of conditions takes three minutes, allowing high throughput evaluation of WER.

WER with different J for $\tau = 3$–20 ns is shown in Fig. 2(a). The increase in τ or J monotonically reduces WER as expected. In the precessional regime, the total amount of transferred angular momentum governs the switching as described earlier and the analytical solution of WER is derived by considering thermal fluctuation at the initial state as[7,12]

$$\mathrm{WER} = 1 - \exp\left\{-4\Delta \exp\left[-2\tau\alpha\gamma\mu_0 H_K^{\mathrm{eff}}\left(\frac{J}{J_{C0}} - \frac{H_z}{H_K^{\mathrm{eff}}} - 1\right)\right]\right\}, \quad (1)$$

where Δ is the thermal stability factor, α is the Gilbert damping constant, γ is the gyromagnetic ratio, μ_0 is the permeability of vacuum, H_K^{eff} is the effective perpendicular anisotropy field, J_{C0} is the intrinsic critical current density, and H_z is the external perpendicular magnetic field. For a constant WER condition, the switching current density J_{th} under $H_z = 0$ is expressed as

$$J_{th} = -\frac{1}{\tau}\frac{J_{C0}}{2\alpha\gamma\mu_0 H_K^{\mathrm{eff}}}\log\left(-\frac{1}{4\Delta\log(\mathrm{WER})}\right) + J_{C0}. \quad (2)$$

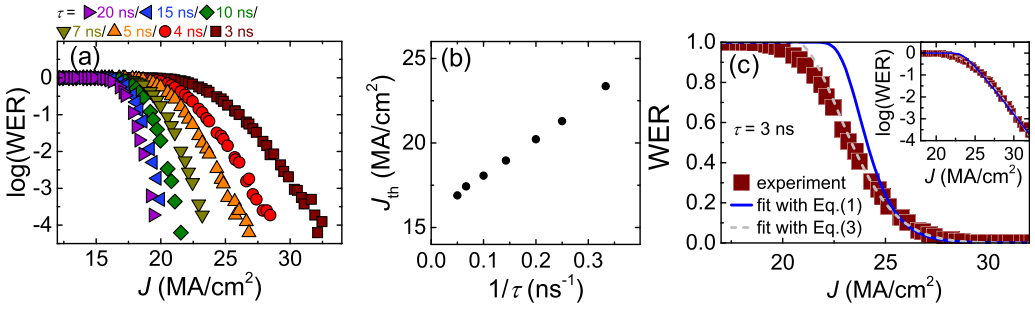

FIG. 2. (a) Write-error rate (WER) as a function of write-current density J for various pulse durations τ. (b) $1/\tau$ dependence of switching current density J_{th}. (c) WER as a function of J with $\tau = 3$ ns. The plot is obtained by experiment. The blue and gray curves are fittings with Eqs. (1) and (3), respectively. The inset shows the same result shown by the logarithmic scale.

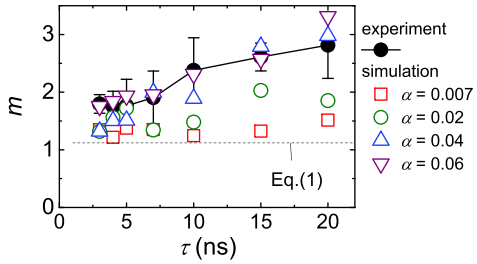

FIG. 3. The nonlinearity index m as a function of pulse duration τ. Experimentally obtained data are plotted by the closed circle. The dashed line and open symbols are obtained by Eq. (1) and macrospin simulation with different τ and damping constants α fitted by Eq. (3), respectively.

Equation (2) indicates a linear relationship between J_{th} and $1/\tau$, with an intercept of J_{C0}. Figure 2(b) shows J_{th} for WER = 0.5 as a function of $1/\tau$. For $\tau < 15$ ns ($1/\tau > 0.07$ ns^{-1}), J_{th} linearly increases with $1/\tau$, in accordance with the analytical model. Next, we compare the model of WER with experiment. The squares in Fig. 2(c) show measured WER as a function of J for $\tau = 3$ ns, whereas the solid (blue) line denotes the fitted curve using Eq. (1), where parameters were adjusted to minimize error on the logarithmic scale (inset). As can be seen in the figure, the fit does not reproduce the experimental results well.

We also note that while Eq. (1) indicates a linear relationship between log(WER) and J at WER $\ll 1$, the experimental results show a nonlinear behavior even at WER $\sim 10^{-3}$. To quantitatively evaluate the degree of nonlinearity, we introduce the following phenomenological equation to approximate the experimental result:

$$\log(\mathrm{WER}) = \begin{cases} 0 & (J < J_1) \\ -C(J - J_1)^m & (J > J_1) \end{cases}, \tag{3}$$

where exponent m denotes a nonlinearity index in WER vs J ($m = 1$ corresponds to a linear relationship), C is a constant, and J_1 is the threshold current density. The result is shown with the dashed (gray) curve in Fig. 2(c), where $m = 1.76$ and $J_1 = 20.9$ MA/cm^2 are obtained by minimizing error on the logarithmic scale for WER $> 10^{-4}$. Figure 3 shows the τ dependence of m (black circle), where m increases with increasing τ. We also plot m obtained by fitting Eqs. (3) to (1) at WER $> 10^{-4}$ by a dashed line, where $m = 1.12$. The gap between the black circles and dashed line indicates that the analytical model is not sufficient for describing WER in this regime.

To probe further, we conduct a numerical simulation based on a macrospin approximation, including the effect of thermal agitation during switching, which is not taken into account in the analytical model. We use the Landau-Lifshitz-Gilbert equation for the polar magnetization angle θ,

$$\frac{\mathrm{d}\theta}{\mathrm{d}t} = \left\{-\alpha\gamma\mu_0 H_K^{\mathrm{eff}} \cos\theta + \tau_{\mathrm{STT}} - \alpha\gamma\mu_0 H_z\right\}\sin\theta + \gamma\mu_0 h_{\mathrm{T},\theta}, \tag{4}$$

where t is the time, $h_{\mathrm{T},\theta}(t)$ is the thermal field with the Gaussian distribution satisfying $\langle h_{\mathrm{T},\theta}(t)\rangle = 0$ and $\langle (h_{\mathrm{T},\theta}(t))^2\rangle = 2\alpha k_B T/\gamma\mu_0 M_S t_{\mathrm{free}} A\Delta t$,[15] τ_{STT} is the STT amplitude given by $\gamma\hbar\mu_0 J g(\theta)/M_S t_{\mathrm{free}}$, $\hbar$ is the Dirac constant, $g(\theta)$ is the spin transfer efficiency determined from the tunnel magnetoresistance (TMR) ratio,[1] $M_S t_{\mathrm{free}}$ is the magnetic moment per unit area (3.3 Tnm, determined by vibrating sample magnetometry), k_B is the Boltzmann constant, Δt is the time step of simulation, and T is the temperature 300 K. $\mu_0 H_K^{\mathrm{eff}}$ is determined to be 350 mT from a switching measurement for MTJs with similar D. θ at $t = 0$ is set to follow the Gaussian distribution with $\langle\theta\rangle = 0$ and $\langle\theta^2\rangle = 1/\{2\Delta(1+H_z/H_K^{\mathrm{eff}})\}$ (see the supplementary material). The first term in Eq. (4) represents the competition of STT with the torque induced by anisotropy and external fields. The second term represents the thermal effect, which increases with α according to fluctuation-dissipation theorem.[15] WER is calculated by computing time evolution of the magnetization vector 2×10^4 times for each τ_{STT}. Each of the initial magnetization directions is obtained by calculating the magnetization trajectory for 20 ns under zero J starting from the energy equilibrium direction. In order to compare the results with experiment, we determine m using Eq. (3) while varying τ_{STT}. The red squares in Fig. 3 are the results using $\alpha = 0.007$, which are obtained from a homodyne-detected ferromagnetic-resonance (FMR) measurement for an MTJ with the same free-layer structure.[16] It is known that the linewidth of FMR for nanoscale MTJ gives a larger value than that of the blanket film due to several extrinsic effects such as the two-magnon scattering and inhomogeneity of anisotropy.[17–19] The value $\alpha = 0.007$ is obtained after excluding these factors by using the perpendicular magnetization configuration and thus represents an intrinsic α.[20,21] The results for $\alpha = 0.02$, 0.04, and 0.06 shown by the circle, triangle, and reversed triangle, respectively, are also included. As can be seen, $\alpha = 0.04$ and 0.06 reproduce the experimental trend well, suggesting that the effective α larger than that of the intrinsic one (=0.007) governs the WER. Note that there are two effects of the damping onto the WER under STT. First, damping changes WER by changing torque against the STT during switching irrespective of thermal agitation, as is expressed in Eqs. (1) and (4). Second, with STT, the magnetization distribution can be different from Boltzmann distribution because the system is not in an equilibrium state. The thermal field is still proportional to the square root of the damping constant;[15] thus, the WER depends on the damping constant.

From Eq. (1), the derivative of log(WER) with respect to H_z in the precessional regime is expressed as

$$\frac{\mathrm{d}\{\log(\mathrm{WER})\}}{\mathrm{d}H_z} = \frac{2\tau\alpha\gamma\mu_0}{\log 10}\frac{x}{\exp(x) - 1}, \tag{5}$$

where $x = 4\Delta\exp\{-2\tau\alpha\gamma\mu_0 H_K^{\mathrm{eff}}(J/J_{C0} - H_z/H_K^{\mathrm{eff}} - 1)\}$. In our experimental condition at WER $< 10^{-2}$, $x \ll 1$ is satisfied and the right-hand side of Eq. (5) converges to $-2\tau\alpha\gamma\mu_0/\log 10$, allowing determination of effective α characterizing WER. Figure 4(a) shows WER vs J at -30 mT $< \mu_0 H_z < 30$ mT and $\tau = 5$ ns. The H_z dependence of WER with various J is shown in Fig. 4(b). We calculate the same dependence using macrospin simulation including thermal agitation. The simulation results with $\alpha = 0.007$ are shown in Fig. 4(c). The slopes that represent the effective damping are different between the experiment and simulation. Figure 4(d) shows the experimental result (closed circles) of the slope $\mathrm{d}\{\log(\mathrm{WER})\}/\mathrm{d}H_z$ at $H_z = 0$ as a function of log(WER) together with the simulation results (open symbols) for various α. The experimental result is again not reproduced by $\alpha = 0.007$ but well by $\alpha = 0.06$ using Eq. (5), consistent with what we found in Fig. 3. The experiment being reproduced by almost an order of magnitude greater α appears to indicate additional relaxation pathways of magnetization dynamics, because the thermal torque increases with α according to the fluctuation-dissipation theorem,[15] which may

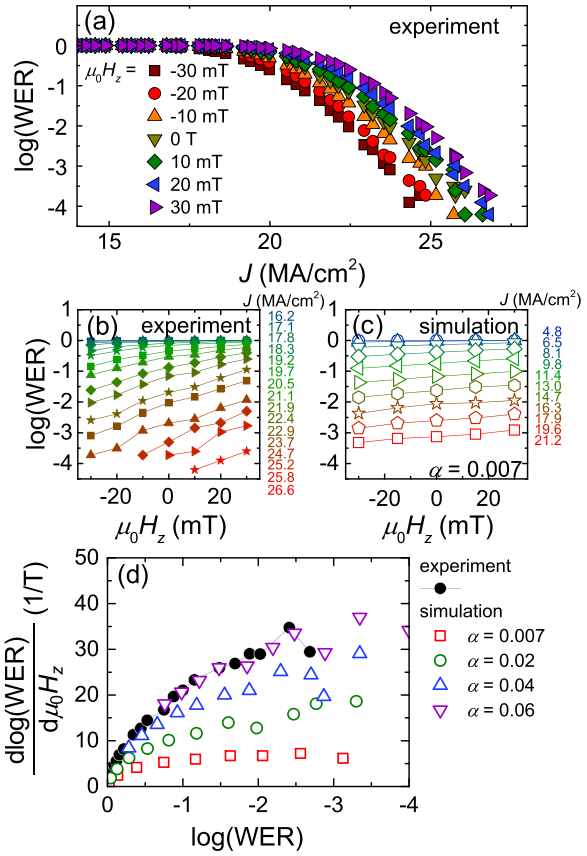

FIG. 4. (a) Experimentally obtained write-error rate (WER) as a function of write-current density J under various magnetic fields H_z with pulse duration $\tau = 5$ ns. (b) and (c) Experimentally obtained (b) and simulated (c) WER as a function of H_z with various J. (d) Slope of log(WER) vs H_z as a function of log(WER).

lead to thermally activated regimelike nonlinear behavior. Note that the derived "effective damping" is a specific damping that characterizes WER. In this regard, the effective damping discussed here could be different from another effective damping that characterizes the figure of merit Δ/I_{c0} and intrinsic damping determined from FMR.[16] One of the possible factors for enhanced relaxation is phase dissipation, which is enhanced with inhomogeneity in the device; e.g., at crystal defect through two-magnon scattering,[19] at the device edge through change of magnetic properties during the process,[22] and at interface of the stack.[23] Enhanced dissipation could result in larger apparent damping through the thermal effect and effective energy relaxation.[24,25] We also note that several studies revealed that the domain wall propagation is a dominant switching mechanism in MTJs with a diameter of down to 40 nm.[26–28] The domain wall width in our device is derived to be 30 nm, which is larger than the diameter of MTJ, suggesting that the macrospin picture should reasonably describe our experiment. WER in the thermally activated regime is confirmed to be well described by the macrospin model as shown in the supplementary material, while, interestingly, WER in the precessional regime is not. This incoherency can also be a factor for the significantly large effective damping as the special incoherency should lead to an energy dissipation. From the application viewpoint, the increase in m in principle improves WER. Our results suggest that even with the fast pulse duration of ~ns, the thermal effect reduces switching error than what is expected from the analytical solution. Simultaneously, however, increasing m leads to read disturbance, an unintentional switching by a read current pulse. Thus, the comprehensive understanding of physics, especially the effective damping, characterizing the STT switching probability in nanoscale MTJs is important to understand and design highly reliable high-speed STT-MRAMs.

In summary, we investigate the write-error rate (WER) in nanoscale perpendicular magnetic tunnel junctions (MTJs) with a diameter of 24 nm for various pulse durations τ down to 3 ns. We measure 1.6×10^4 switching events using an arbitrary waveform generator and high-speed oscilloscope. WER as a function of current density J, τ, and magnetic field H_z is compared with the analytical solution and macrospin simulation. While the switching current density J_{th} shows a linear dependence on $1/\tau$ for $\tau < 15$ ns, which is a typical characteristic of the precessional regime, log(WER) vs J is not reproduced by the corresponding analytical solution. The measurement of WER under H_z reveals that WER is characterized by an apparent damping constant $\alpha \simeq 0.06$, with which the experimental results are well described. The larger value of apparent damping than the intrinsic one suggests an enhanced relaxation rate and/or thermal effect.

See the supplementary material for the WER in the thermally activated regime and the thermal field in the LLG equation.

The authors thank S. Kubota, N. Ohshima, T. Funatsu, J. Igarashi, Y. Takeuchi, T. Hirata, I. Morita, H. Iwanuma, and K. Goto for discussion and technical support. This work was supported in part by the ImPACT Program of CSTI, JST-OPERA Program Grant No. JPMJOP1611, JSPS Kakenhi No. 19H05622, Core-to-Core Program of JSPS, and Cooperative Research Projects of RIEC.

REFERENCES

[1] J. C. Slonczewski, J. Magn. Magn. Mater. **159**, L1 (1996).
[2] L. Berger, Phys. Rev. B **54**, 9353 (1996).
[3] S. Ikeda, K. Miura, H. Yamamoto, K. Mizunuma, H. D. Gan, M. Endo, S. Kanai, J. Hayakawa, F. Matsukura, and H. Ohno, Nat. Mater. **9**, 721 (2010).
[4] A. Brataas, A. D. Kent, and H. Ohno, Nat. Mater. **11**, 372 (2012).
[5] Y. Xie, B. Behin-Aein, and A. W. Ghosh, IEEE Trans. Electron Devices **64**, 319 (2017).
[6] W. H. Butler, T. Mewes, C. K. A. Mewes, P. B. Visscher, W. H. Rippard, S. E. Russek, and R. Heindl, IEEE Trans. Magn. **48**, 4684 (2012).
[7] H. Liu, D. Bedau, J. Z. Sun, S. Mangin, E. E. Fullerton, J. A. Katine, and A. D. Kent, J. Magn. Magn. Mater. **358–359**, 233 (2014).
[8] T. Taniguchi, Y. Utsumi, M. Marthaler, D. S. Golubev, and H. Imamura, Phys. Rev. B **87**, 054406 (2013).
[9] J. J. Nowak, R. P. Robertazzi, J. Z. Sun, G. Hu, D. W. Abraham, P. L. Trouilloud, S. Brown, M. C. Gaidis, E. J. O'Sullivan, W. J. Gallagher, and D. C. Worledge, IEEE Magn. Lett. **2**, 3000204 (2011).
[10] R. Robertazzi, J. J. Nowak, and J. Z. Sun, Int. Test Conf. **1–10**, 23.2 (2014).
[11] J. J. Nowak, R. P. Robertazzi, J. Z. Sun, G. Hu, J.-H. Park, J. Lee, A. J. Annunziata, G. P. Lauer, R. Kothandaraman, E. J. O'Sullivan, P. L. Trouilloud, Y. Kim, and D. C. Worledge, IEEE Magn. Lett. **7**, 1 (2016).
[12] G. Jan, Y.-J. Wang, T. Moriyama, Y.-J. Lee, M. Lin, T. Zhong, R.-Y. Tong, T. Torng, and P.-K. Wang, Appl. Phys. Express **5**, 093008 (2012).
[13] R. H. Koch, J. A. Katine, and J. Z. Sun, Phys. Rev. Lett. **92**, 088302 (2004).

[14]H. Sato, E. C. I. Enobio, M. Yamanouchi, S. Ikeda, S. Fukami, S. Kanai, F. Matsukura, and H. Ohno, Appl. Phys. Lett. **105**, 062403 (2014).
[15]W. F. Brown, Phys. Rev. **130**(5), 1677–1686 (1963).
[16]M. Shinozaki, E. Hirayama, S. Kanai, H. Sato, F. Matsukura, and H. Ohno, Appl. Phys. Express **10**, 013001 (2017).
[17]E. Hirayama, S. Kanai, H. Sato, F. Matsukura, and H. Ohno, J. Appl. Phys. **117**, 17B708 (2015).
[18]T. Nozaki, Y. Shiota, S. Miwa, S. Murakami, F. Bonell, S. Ishibashi, H. Kubota, K. Yakushiji, T. Saruya, A. Fukushima, S. Yuasa, T. Shinjo, and Y. Suzuki, Nat. Phys. **8**, 491 (2012).
[19]R. Arias and D. L. Mills, Phys. Rev. B **60**, 7395 (1999).
[20]M. A. W. Schoen, J. Lucassen, H. T. Nembach, B. Koopmans, T. J. Silva, C. H. Back, and J. M. Shaw, Phys. Rev. B **95**, 134411 (2017).
[21]J. M. Shaw, E. K. Delczeg-Czirjak, E. R. J. Edwards, Y. Kvashnin, D. Thonig, M. A. W. Schoen, M. Pufall, M. L. Schneider, T. J. Silva, O. Karis, K. P. Rice, O. Eriksson, and H. T. Nembach, Phys. Rev. B **97**, 094420 (2018).
[22]M. Shinozaki, J. Igarashi, H. Sato, and H. Ohno, Appl. Phys. Express **11**, 043001 (2018).
[23]A. Okada, S. He, B. Gu, S. Kanai, A. Soumyanarayanan, S. T. Lim, M. Tran, M. Mori, S. Maekawa, F. Matsukura, H. Ohno, and C. Panagopoulos, Proc. Nat. Acad. Sci. U.S.A. **114**, 3815–3820 (2017).
[24]J. Xiao, G. E. W. Bauer, K. Uchida, E. Saitoh, and S. Maekawa, Phys. Rev. B **81**, 214418 (2010).
[25]J. Z. Sun, R. P. Robertazzi, J. Nowak, P. L. Trouilloud, G. Hu, D. W. Abraham, M. C. Gaidis, S. L. Brown, E. J. O'Sullivan, W. J. Gallagher, and D. C. Worledge, Phys. Rev. B **84**, 064413 (2011).
[26]J. Cucchiara, S. Le Gall, E. E. Fullerton, J.-V. Kim, D. Ravelosona, Y. Henry, J. A. Katine, A. D. Kent, D. Bedau, D. Gopman, and S. Mangin, Phys. Rev. B **86**, 214429 (2012).
[27]T. Devolder, A. Le Goff, and V. Nikitin, Phys. Rev. B **93**, 224432 (2016).
[28]T. Devolder, J.-V. Kim, J. Swerts, W. Kim, S. Couet, G. Kar, A. Furnemont, and V. Nikitin, IEEE Trans. Magn. **54**, 3400109 (2018).